Hindawi
Shock and Vibration
Volume 2022, Article ID 6369832, 17 pages
https://doi.org/10.1155/2022/6369832

Research Article

Analysis of the Vibro-Acoustic Behavior of a Stiffened Double Panel-Cavity System

Na Wang,[1] Mingfei Chen ,[2] Yantao Zhang,[3] Shuangxia Shi,[4] Guoyong Jin,[1] and Zhigang Liu[1]

[1]*College of Power and Energy Engineering, Harbin Engineering University, Harbin 150001, China*
[2]*School of Mechanical Engineering, Guizhou University, Guizhou 550025, China*
[3]*PLA Unit 92578, Beijing 100000, China*
[4]*School of Energy and Power Engineering, Northeast Electric Power University, Jilin 132012, China*

Correspondence should be addressed to Mingfei Chen; sowstone@163.com

Received 4 September 2021; Revised 8 April 2022; Accepted 16 June 2022; Published 11 July 2022

Academic Editor: Yuxing Li

An analytical solution for the vibro-acoustic behavior analysis of a stiffened double panel-cavity coupled system is presented. Unlike existing methods, this method is flexible with parameter analysis and can simulate the elastic boundary conditions of a stiffened double panel structure. The displacements of the stiffened double panel structures and the sound pressure of two inner acoustic cavities are expressed by two-dimensional (2D) and three-dimensional (3D) improved Fourier series methods, respectively. Then, the unknown coefficients of the vibro-acoustic control equation are solved by the Rayleigh–Ritz method based on the virtual works principle applied to the coupled system. In numerical results, the accuracy and effectiveness of the proposed method are validated by several comparison examples. Finally, the influence of some parameters on the vibro-acoustic behavior of the coupled system is investigated. Numerical results show that the external acoustic excitation at a certain angle can stimulate more resonant responses of the panel-cavity coupled system. This work can predict quickly the vibro-acoustic behavior of the stiffened double panel-cavity coupled system with a small truncation number. Some new results can be used as reference data for future work.

1. Introduction

Stiffened double panel-cavity coupled systems are widely used in engineering applications, such as transportation systems, aircraft fuselage shells, modern buildings, window glazing, and vehicles, due to their good sound insulation, heat preservation characteristics, and good rigidity. The study of the vibro-acoustic behavior of stiffened double panel-cavity coupled systems has been an important research topic in vibration and acoustic fields.

In the double panel-cavity coupled system, not only the vibration of the plates [1–7] and the sound pressure of the cavity [8–11] but also the coupled characteristics of the plate with the cavity should be considered. To provide some helpful insights into the sound transmission and energy transmission mechanism, some researchers made sufficient efforts [12–17] for panel-cavity coupled systems in the last few decades.

Research on double panel-cavity coupled systems attracted more attention from engineers. Kam et al. [18] investigated the vibro-acoustic characteristics of the acoustic cavity enclosed by a shear-deformed plate under elastic boundary conditions with the first Rayleigh integral and Rayleigh–Ritz method. Carneal and Fuller [19] used the experimental method to study the active control of sound transmission in a double panel-cavity system and then revealed the transmission mechanism of sound radiation in a double panel-cavity system. Xin et al. [20] used the Fourier series with the weighted residual method to study the vibro-acoustic characteristics of a double panel-cavity system with clamped boundary conditions. In the following work, they continued to study the sound transmission of a double

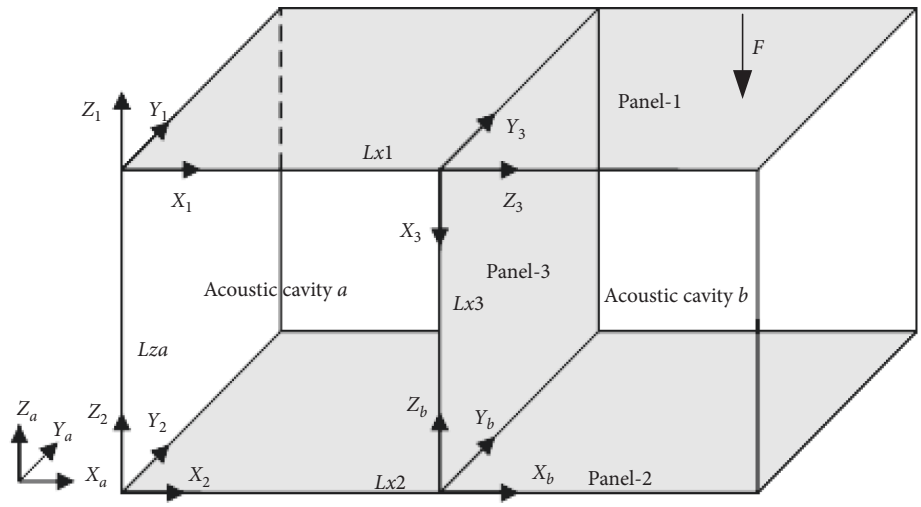

Figure 1: Schematic of the stiffened double panel-cavity coupled system model.

panel-cavity system with simply supported boundary conditions [21]. Raviprolu et al. [22] established an analytical model for the sound radiation behavior of a rectangular duct with flexible walls. Guo et al. [23] used the temperature field theory and modal superposition method to investigate the vibro-acoustic behavior of simply supported double partitions in a thermal environment. Lee [24] applied the multilevel residue harmonic balance method to establish the free vibration behavior analysis model of a nonlinear panel coupled with an extended cavity. Sadri and Younesian [25] studied the free vibration of a plate-cavity coupled system based on the Von Karman plate theory.

It is worth noting that the above-mentioned contributions to the vibro-acoustic behavior of plate-cavity coupled systems are limited to classical boundary conditions. To consider the elastically restrained boundary conditions of structures and the general impedance boundary conditions of a cavity, the improved Fourier series method was used by many researchers. Zhang and Li [26] adopted this method to analyze the vibration of a rectangular plate with arbitrary nonuniform elastic edge restraints. Chen et al. [27] used also this method to analyze the vibration and energy transmission characteristics of a plate structure with elastic edge restraints. Du et al. [28] solved the general impedance boundary condition simulation problem of a rectangular acoustic cavity by the improved Fourier series method; later, they established the vibro-acoustic analysis model of a panel-cavity coupled system [29]. Shi et al. [30] used this method to analyze the acoustic modals and steady-state responses of triangular and quadrangular prism acoustic cavities. Zhang et al. [31] used this method to analyze the vibro-acoustic analysis of an annular segment flexible panel-cavity coupled system. Shi et al. [32] used this improved Fourier series method to establish the theoretical model of a double panel-cavity coupled system and analyzed their vibro-acoustic behavior and sound transmission loss.

However, to the best of the authors' knowledge, there is no related research on the acoustic and vibration characteristics of the stiffened double panel-cavity coupled system with elastically restrained boundary conditions. Therefore, it is very necessary to establish the vibro-acoustic model of stiffened double panel-cavity coupled system and analyze their acoustic and vibration characteristics. In this paper, the improved Fourier series method [33] is used to describe the displacement functions of the plate structure and the sound pressure functions in the acoustic cavity. Then the energy principle is introduced for coupled energy in panel-panel and panel-cavity coupled positions. Finally, the Rayleigh–Ritz method is used to solve the unknown coefficient of the equations. In numerical results, the accuracy of this method is verified comparison with the results obtained by the finite element method.

2. Theoretical Formulations

2.1. Description of the Coupled System. Consider the stiffened double panel-cavity coupled system model that is a composite of two enclosed cavities and three thin panels, as shown in Figure 1. To simplify the description, the coordinate systems and notations of the stiffened double panel-cavity coupled system are defined in Figure 1. Panels 1 and 2 represent the incident panel and the radiating panel, respectively. Panel 3 denotes the stiffener that is coupled with panels 1 and 2. The acoustic cavity a and acoustic cavity b are enclosed by these panels.

The boundary and structural coupled conditions of the system can be described in the form of elastic springs shown in Figure 2. The stiffness coefficients of normal and tangential springs can be represented by the symbols k and K, respectively. Then arbitrary boundary conditions and arbitrary coupled conditions can be obtained by setting these boundary springs and coupled springs as appropriate values. For example, setting the stiffness coefficients of boundary springs of four sides to infinity (5e9) represents that four sides of the panel are clamped (CCCC). In the same way, the free boundary of four sides (FFFF) denotes setting the stiffness coefficients of boundary springs as zero. Except for these coupled interfaces in the panel-cavity coupled systems,

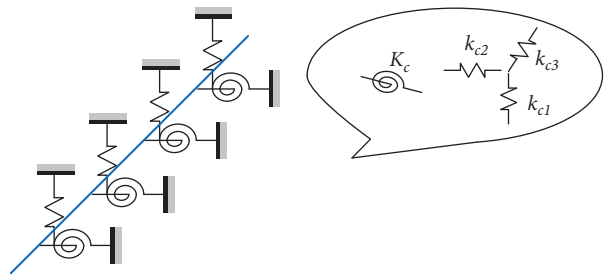

Figure 2: Boundary spring and coupled spring at: (a) the boundary position and (b) the coupled position.

other acoustic boundaries of the acoustic cavity a and b are considered rigid walls.

2.2. Vibration and Acoustic Equations of the Coupled System. In this paper, the displacement functions of each panel and the acoustic pressure functions of each acoustic cavity can be described by two- and three-dimensional improved methods [33], respectively. For the sake of convenience and simplicity, only the examples using the improved Fourier method to describe panel 1 and acoustic cavity a are given here.

The displacement functions of the panel 1 can be expressed as follows:

$$\begin{aligned} w_1(x_1, y_1) = &\sum_{m=0}^{\infty}\sum_{n=0}^{\infty} A_{1\,\mathrm{mn}}\cos(\lambda_{\mathrm{mLx}\,1}x_1)\cos(\lambda_{\mathrm{nLy}\,1}y_1) \\ &+ \sum_{m=0}^{\infty}\sum_{k=1}^{4} a_{1\,\mathrm{km}}\zeta_{\mathrm{kLy}\,1}(y_1)\cos(\lambda_{\mathrm{mLx}\,1}x_1) \\ &+ \sum_{n=0}^{\infty}\sum_{k=1}^{4} \overline{a}_{1\,\mathrm{kn}}\zeta_{\mathrm{kLx}\,1}(x_1)\cos(\lambda_{\mathrm{nLy}\,1}y_1), \end{aligned} \tag{1}$$

$$\begin{aligned} u_1(x_1, y_1) = &\sum_{m=0}^{\infty}\sum_{n=0}^{\infty} B_{1\,\mathrm{mn}}\cos(\lambda_{\mathrm{mLx}\,1}x_1)\cos(\lambda_{\mathrm{nLy}\,1}y_1) \\ &+ \sum_{n=0}^{\infty}\sum_{k=1}^{2} b_{1\,\mathrm{kn}}\xi_{\mathrm{kLx}\,1}(x_1)\cos(\lambda_{\mathrm{nLy}\,1}y_1) \\ &+ \sum_{m=0}^{\infty}\sum_{k=1}^{2} \overline{b}_{1\,\mathrm{km}}\xi_{\mathrm{kLy}\,1}(y_1)\cos(\lambda_{\mathrm{mLx}\,1}x_1), \end{aligned} \tag{2}$$

$$\begin{aligned} v_1(x_1, y_1) = &\sum_{m=0}^{\infty}\sum_{n=0}^{\infty} C_{1\,\mathrm{mn}}\cos(\lambda_{\mathrm{mLx}\,1}x_1)\cos(\lambda_{\mathrm{nLy}\,1}y_1) \\ &+ \sum_{n=0}^{\infty}\sum_{k=1}^{2} c_{1\,\mathrm{kn}}\xi_{\mathrm{kLx}\,1}(x_1)\cos(\lambda_{\mathrm{nLy}\,1}y_1) \\ &+ \sum_{m=0}^{\infty}\sum_{k=1}^{2} \overline{c}_{1\,\mathrm{km}}\xi_{\mathrm{kLy}\,1}(y_1)\cos(\lambda_{\mathrm{mLx}\,1}x_1), \end{aligned} \tag{3}$$

where $\lambda_{\mathrm{mLx}\,1} = m\pi/\mathrm{Lx}\,1$ and $\lambda_{\mathrm{nLy}\,1} = n\pi/\mathrm{Ly}\,1$. $A_{1\,\mathrm{mn}}$, $a_{1\,\mathrm{km}}$, and $\overline{a}_{1\,\mathrm{kn}}$ represent the unknown coefficients of the bending displacement; $B_{1\,\mathrm{mn}}$, $b_{1\,\mathrm{kn}}$, $\overline{b}_{1\,\mathrm{km}}$, $C_{1\,\mathrm{mn}}$, $c_{1\,\mathrm{kn}}$, and $\overline{c}_{1\,\mathrm{km}}$ represent the unknown coefficients of in-plane displacement. $\zeta_{\mathrm{kLy}\,1}(y_1)$ and $\zeta_{\mathrm{kLx}\,1}$ represent the supplementary functions of the bending displacement. $\xi_{\mathrm{kLx}\,1}(x_1)$ and $\xi_{\mathrm{kLy}\,1}(y_1)$ represent the supplementary functions of the in-plane displacement. These supplementary functions are introduced to overcome the discontinuities with the displacement function and their partial derivatives at the boundary and coupled position of the panel. Considering computer speed, property truncation numbers M and N should be selected in the actual calculation.

Similarly, the acoustic pressure functions of the acoustic cavity a can be expressed as follows:

$$\begin{aligned} p_a(x_a, y_a, z_a) = &\sum_{m_x=0}^{\infty}\sum_{m_y=0}^{\infty}\sum_{m_z=0}^{\infty} A_{\mathrm{am}_x m_y m_z}\cos(\lambda_{m_x\,\mathrm{Lxa}}x_a) \\ &\cos(\lambda_{m_y\,\mathrm{Lya}}y_a)\cos(\lambda_{m_z\,\mathrm{Lza}}z_a) \\ &+ \sum_{m_x=0}^{\infty}\sum_{k=1}^{2} a_{\mathrm{akm}_x m_y}\xi_{\mathrm{kLza}}(z_a)\cos(\lambda_{m_x\,\mathrm{Lxa}}x_a)\cos(\lambda_{m_y\,\mathrm{Lya}}y_a) \\ &+ \sum_{m_x=0}^{\infty}\sum_{k=1}^{2} b_{\mathrm{akm}_x m_z}\xi_{\mathrm{kLya}}(y_a)\cos(\lambda_{m_x\,\mathrm{Lxa}}x_a)\cos(\lambda_{m_z\,\mathrm{Lza}}z_a) \\ &+ \sum_{m_y=0}^{\infty}\sum_{k=1}^{2} c_{\mathrm{akm}_y m_z}\xi_{\mathrm{kLxa}}(x_a)\cos(\lambda_{m_y\,\mathrm{Lya}}y_a)\cos(\lambda_{m_z\,\mathrm{Lza}}z_a), \end{aligned} \tag{4}$$

where $\lambda_{m_x\,\mathrm{Lxa}} = m_x\pi/\mathrm{Lxa}$, $\lambda_{m_y\,\mathrm{Lxa}} = m_y\pi/\mathrm{Lya}$, and $\lambda_{m_z\,\mathrm{Lxa}} = m_z\pi/\mathrm{Lza}$. $A_{\mathrm{am}_x m_y m_z}$, $a_{\mathrm{akm}_x m_y}$, $b_{\mathrm{akm}_x m_z}$, and $c_{\mathrm{akm}_y m_z}$ represent the unknown coefficients of the acoustic pressure. $\xi_{\mathrm{kLza}}(z_a)$, $\xi_{\mathrm{kLya}}(y_a)$, and $\xi_{\mathrm{kLxa}}(x_a)$ represent the supplementary functions of the acoustic pressure. Property truncation numbers M_x, M_y, and M_z should be selected in the actual calculation.

The vibro-acoustic equations of the stiffened double panel-cavity coupled system can be written by the energy principle. The Lagrangian of the stiffened double panel structure and two acoustic cavities can be expressed as follows:

$$L_s = U_s - T_s + W_s + W_{\mathrm{ca}\,\&s} + W_{\mathrm{cb}\,\&s}, \tag{5}$$

$$L_{a-c} = U_{a-c} - T_{a-c} + W_{a-\mathrm{ext}}. \tag{6}$$

$$L_{b-c} = U_{b-c} - T_{b-c} + W_{b-\mathrm{ext}}, \tag{7}$$

where U_s is the total potential energy of the stiffened double panel structure, including the bending and in-plane

potential energy of panels, the potential energy of boundary springs, and the potential energy of the coupled springs at the structural coupled positions. T_s is the total kinetic energy of stiffened double panel structure. $W_{\mathrm{ca}\,\&s}$ and $W_{\mathrm{cb}\,\&s}$ are the work done by the acoustic cavities a and b acting on the panel-cavity coupled interface. W_s is the total work done by the external force. U_{a-c} and T_{a-c} are the potential and kinetic energy of acoustic cavity a, respectively. $W_{a-\mathrm{ext}}$ is the energy exchange between the outside parts with acoustic cavity a, including the work done by the wall surfaces, the work done by the sound source in the acoustic cavity a, and the energy exchange on the panel-cavity coupled surface. The mean of the expressions in equation (7) is similar to the one in equation (6).

These explicit energy and work expressions in the above equations can be expressed as follows:

$$W_s = -\mathrm{Fw}_1(x_e, y_e), \tag{8}$$

$$W_{\mathrm{ca}\,\&s} = \iint_s \mathrm{wp}_a \mathrm{d}s, \tag{9}$$

$$U_s = \sum_{j=1}^{3} U_{\mathrm{jb}} + \sum_{j=1}^{3} U_{\mathrm{ji}} + \sum_{q=1}^{2} U_{\mathrm{qc}} + \sum_{r=1}^{12} U_{\mathrm{rs}}, \tag{10}$$

$$T_s = \sum_{j=1}^{3} T_{\mathrm{jb}} + \sum_{j=1}^{3} T_{\mathrm{ji}}, \tag{11}$$

$$W_{a-\mathrm{ext}} = W_{s\&\mathrm{ca}} + W_{\mathrm{awall}} + W_{\mathrm{as}}, \tag{12}$$

where U_{jb} and U_{ji} denote the bending and in-plane potential energy of the panel j structure, respectively. T_{jb} and T_{ji} denote the bending and in-plane kinetic energy of the panel j structure, respectively. U_{qc} denotes the potential energy of the coupled spring at the q-th panel-panel coupled position. U_{rs} denotes the potential energy of the boundary spring at the rth side of the stiffened double panel structure. $W_{s\&\mathrm{ca}} = -W_{\mathrm{ca}\,\&s}$ denotes the work done by the stiffened double panel structure on the acoustic cavity a. $W_{\mathrm{awall}} = 0$ and $W_{\mathrm{as}} = 0$ denote the work done by the sound source in cavity a and the impedance wall surfaces, respectively.

The potential and kinetic energy of the panel j structure can be expressed as follows:

$$U_{\mathrm{jb}} = \frac{D_j}{2}\int_0^{\mathrm{Lyj}}\int_0^{\mathrm{Lxj}} \left(\frac{\partial^2 w_j}{\partial x_j^2}\right)^2 + \left(\frac{\partial^2 w_j}{\partial y_j^2}\right)^2 + 2\mu_j \frac{\partial^2 w_j}{\partial x_j^2}\frac{\partial^2 w_j}{\partial y_j^2} + 2(1-\mu_j)\left(\frac{\partial^2 w_j}{\partial x_j \partial y_j}\right)^2 \mathrm{d}x_j \mathrm{d}y_j, \tag{13}$$

$$U_{\mathrm{ji}} = \frac{G_j}{2}\int_0^{\mathrm{Lyj}}\int_0^{\mathrm{Lxj}} \left(\frac{\partial u_j}{\partial x_j} + \frac{\partial v_j}{\partial y_j}\right)^2 - 2(1-\mu_j)\frac{\partial u_j}{\partial x_j}\frac{\partial v_j}{\partial y_j} + \frac{(1-\mu_j)}{2}\left(\frac{\partial v_j}{\partial x_j} + \frac{\partial u_j}{\partial y_j}\right)^2 \mathrm{d}x_j \mathrm{d}y_j, \tag{14}$$

$$T_{\mathrm{jb}} = \frac{1}{2}\rho_j h_j \omega^2 \int_0^{\mathrm{Lyj}}\int_0^{\mathrm{Lxj}} w_j^2 \mathrm{d}x_j \mathrm{d}y_j, \tag{15}$$

$$T_{\mathrm{ji}} = \frac{1}{2}\rho_j h_j \omega^2 \int_0^{\mathrm{Lyj}}\int_0^{\mathrm{Lxj}} \left[u_j^2 + v_j^2\right] \mathrm{d}x_j \mathrm{d}y_j, \tag{16}$$

where D_j and G_j represent the bending and stretching stiffness of panel j structure, respectively. ρ_j, h_j, and μ_j represent the density, thickness, and Poisson's ratio of the panel j structure, respectively. ω denotes the angular frequency of the system.

The coupled potential energy of the first structural coupled position and the boundary potential energy of the first boundary can be written as follows:

$$U_{1c} = \frac{1}{2}\int_0^{\mathrm{Ly}1} K_{c1}\left(\partial w_1/\partial x_1|_{x_1=Lx1c} - \partial w_2/\partial x_2|_{x_2=\mathrm{Lx}2}\right)^2 + k_{c1}\left(w_1|_{x_1=\mathrm{Lx}1c} + u_2|_{x_2=\mathrm{Lx}2}\right)^2 + k_{c2}\left(u_1|_{x_1=\mathrm{Lx}1c} - w_2|_{x_2=\mathrm{Lx}2}\right)^2 + k_{c3}\left(v_1|_{x_1=\mathrm{Lx}1c} - v_2|_{x_2=\mathrm{Lx}2}\right)^2 \mathrm{d}y_1, \tag{17}$$

$$U_{1s} = \int_0^{L1} k_{w1} w_1^2 + K_{w1}\left(\frac{\partial w_1}{\partial x_1}\right)^2 + k_{n1} u_1^2 + k_{p1} v_1^2 \mathrm{d}y_1, \tag{18}$$

where k_{c1}, k_{c2}, k_{c3}, and K_{c1} represent the stiffness coefficients of coupled springs. k_{w1}, k_{n1}, k_{p1}, and K_{w1} represent the stiffness coefficients of boundary springs. Spring symbols K and k denote tangential and normal springs, respectively. $Lx1c$ represents the coupled position in the panel 1 structure. The subscript 1 of the displacement and the coordinate symbols denotes the panel 1 structure. Other coupled potential energy of the first coupled position and the boundary potential energy can be obtained by changing corresponding subscripts. Through setting stiffness coefficients to each spring of these panels, different boundary and structure coupled conditions can be obtained. For example, the classical boundary conditions of the panel, clamped (C), free (F), and simply supported (S) boundary conditions can be easily realized by setting the stiffness of springs as proper values:

at the edge $x_1 = 0$ or $x_1 = Lx1$,

$$\begin{cases} u = v = w = \varphi_x = \varphi_y = 0, & \text{for } C \\ N_x = N_{\mathrm{xy}} = Q_x = M_x = M_{\mathrm{xy}} = 0, & \text{for } F, \\ u = w = \varphi_x = 0, N_{\mathrm{xy}} = M_{\mathrm{xy}} = 0, & \text{for S} \end{cases} \tag{19}$$

at the edge $y_1 = 0$ or $y_1 = Ly1$,

$$\begin{cases} u = v = w = \varphi_x = \varphi_y = 0, & \text{for } C \\ N_x = N_{\mathrm{xy}} = Q_x = M_x = M_{\mathrm{xy}} = 0, & \text{for } F \\ v = w = \varphi_y = 0, \quad N_{\mathrm{xy}} = M_{\mathrm{xy}} = 0, & \text{for } S \end{cases} \tag{20}$$

The potential and kinetic energy of the acoustic cavity a can be expressed as follows:

$$U_{a-c} = \frac{1}{2\rho_a c_a^2}\int_{V_a} p_a^2 \mathrm{d}V_a. \tag{21}$$

$$T_{a-c} = \frac{1}{2\rho_a \omega^2}\int_{V_a}\left[\left(\frac{\partial p_a}{\partial x_a}\right)^2 + \left(\frac{\partial p_a}{\partial y_a}\right)^2 + \left(\frac{\partial p_a}{\partial z_a}\right)^2\right]\mathrm{d}V_a, \tag{22}$$

where V_a denotes the volume of acoustic cavity a. p_a is the sound pressure in acoustic cavity a. ρ_a is the density of acoustic cavity a. c_a is the acoustic velocity of cavity a. The total work of acoustic cavity a to the stiffened double panel structure can be expressed as follows:

$$W_{\mathrm{ca}\,\&s} = W_{\mathrm{ca}\,\&p1} + W_{\mathrm{ca}\,\&p2} + W_{\mathrm{ca}\,\&p3}. \tag{23}$$

and

$$\begin{cases} W_{\mathrm{ca}\,\&p1} = \int_0^{\mathrm{Lya}}\int_0^{\mathrm{Lxa}} w_1 p_a \mathrm{d}x_a \mathrm{d}y_a, \\ W_{\mathrm{ca}\,\&p2} = -\int_0^{\mathrm{Lya}}\int_0^{\mathrm{Lxa}} w_2 p_a \mathrm{d}x_a \mathrm{d}y_a, \\ W_{\mathrm{ca}\,\&p3} = \int_0^{\mathrm{Lza}}\int_0^{\mathrm{Lya}} w_3 p_a \mathrm{d}y_a \mathrm{d}z_a, \end{cases} \tag{24}$$

where *Lxa*, *Lya*, and *Lza* represent the length, width, and height of the acoustic cavity a, respectively. w_1, w_2, and w_3 represent the bending displacements of panels 1, 2, and 3. The kinetic energy, the potential energy of acoustic cavity b, and the total work done on the stiffened double panel structure system can be obtained by changing corresponding subscripts in equations (21)–(24).

As above description, the Lagrange function equations of the stiffened double panel-cavity coupled system can be determined by the energy expressions of the acoustic cavity a, the acoustic cavity b, and the stiffened double panel structures. Substituting the displacement and sound pressure functions in equations (1)–(4) into the Lagrangian function equations in equations (5)–(7) and then using the Rayleigh–Ritz method against each unknown Fourier coefficient of the vibro-acoustic equations, the following matrix forms can be obtained:

$$\left\{\begin{bmatrix} \mathbf{K}_s & \mathbf{C}_{a\&s} & \mathbf{C}_{b\&s} \\ 0 & \mathbf{K}_a & 0 \\ 0 & 0 & \mathbf{K}_b \end{bmatrix} - \omega^2 \begin{bmatrix} \mathbf{M}_p & 0 & 0 \\ \mathbf{C}_{s\&a} & \mathbf{M}_a & 0 \\ \mathbf{C}_{s\&b} & 0 & \mathbf{M}_b \end{bmatrix}\right\}\begin{bmatrix} \mathbf{E} \\ \mathbf{P}_a \\ \mathbf{P}_b \end{bmatrix} = \begin{Bmatrix} \mathbf{F}_s \\ 0 \\ 0 \end{Bmatrix}, \tag{25}$$

where $\mathbf{K}_s$ and $\mathbf{M}_p$ denote the stiffness and mass matrices of the stiffened double panel structure, respectively. $\mathbf{K}_a$ and $\mathbf{M}_a$ denote the stiffness and mass matrices of the acoustic cavity a, respectively. $\mathbf{K}_b$ and $\mathbf{M}_b$ denote the stiffness and mass matrices of the acoustic cavity b, respectively. $\mathbf{C}_{s\&a} = -\mathbf{C}_{a\&s}^{\mathrm{T}}$ and $\mathbf{C}_{s\&b} = -\mathbf{C}_{b\&s}^{\mathrm{T}}$ denote the panel-cavity coupled matrices for the stiffened double panel structure acting on the acoustic cavity a and b, respectively. ω denotes the angular frequency of the system. $\mathbf{P}_a$, $\mathbf{P}_b$, and $\mathbf{E}$ denote the unknown Fourier coefficients of the sound pressure inner acoustic cavities and the displacements of all panels. The free vibro-acoustic behavior of this system can be obtained by setting the force vector at the right end of equation (25) to the zero vector.

2.3. Sound Transmission Loss. The incident acoustic power can be written as follows:

$$\prod_{\mathrm{in}} = \frac{1}{2}\mathrm{Re}\iint_A p_i v_i^* \mathrm{d}A, \tag{26}$$

where symbol p_i denotes the incident sound pressure and $v_i = p_i/(\rho_{\mathrm{air}} c_{\mathrm{air}})$ is the acoustic velocity. Item marked with an asterisk denotes the complex conjugate. ρ_{air} and c_{air} denote the density and acoustic velocity of air, respectively. When the incident wave is plane, the incident acoustic power in equation (26) can be also written as follows:

$$\prod_{\mathrm{in}} = \frac{p_i^2 \cdot \cos(\varphi) \cdot \mathrm{Lx}\,1 \cdot \mathrm{Ly}\,1}{2\rho_{\mathrm{air}} c_{\mathrm{air}}}, \tag{27}$$

where φ is the incident elevation angle.

The radiated acoustic power from the radiating panel can be written as follows:

$$\prod_{r} = \frac{1}{2}\mathrm{Re}\iint_A p_r v_r^* \mathrm{d}A, \tag{28}$$

where v_r and p_r denote the acoustic velocity and sound pressure on the surface of the radiating panel, respectively. The expression of v_r can be written as follows:

$$v_r = j \cdot \omega \cdot w_2(x, y). \tag{29}$$

On the basis of Rayleigh's integral, the sound pressure on the radiating panel p_r can be written as follows:

$$p_r = \frac{j \cdot k \cdot \rho_{\mathrm{air}} \cdot c_{\mathrm{air}}}{2 \cdot \pi}\iint_s v_r(x, y)\frac{e^{-j\cdot k\cdot r}}{r}\mathrm{d}s, \tag{30}$$

where $k = \omega/c_{\mathrm{air}}$ denotes the wave number. r is the distance between the sound pressure point and the vibration source.

Substituting the acoustic velocity on the radiating panel v_r in equation (29) and the sound pressure on the radiating panel p_r in equation (30) into equation (28), the radiated acoustic power can be expressed as follows:

$$\prod_{r} = \frac{\rho_{\mathrm{air}} c_{\mathrm{air}}}{2}\mathrm{Re}\left[\iint_s \frac{j\cdot k}{2\pi}\iint_s v_r(x_s, y_s)\frac{e^{-j\cdot k\cdot r}}{r}v_r^*(x, y)\mathrm{d}s\mathrm{d}s\right], \tag{31}$$

After dividing the surface S of the radiating panel into discrete elements S_m ($m = 1,2, \cdots M_s$), the discrete distribution of the radiated acoustic power can be written as follows:

$$\begin{aligned} \prod_{r} &= \frac{\rho_{\mathrm{air}} c_{\mathrm{air}}}{2}\frac{k^2}{2\pi}\sum_{m=1}^{M_s}\sum_{n=1}^{M_s}\iint_{s_n}\iint_{s_m} v_{r_m}\frac{\sin(k\cdot r_{mn})}{k\cdot r_{mn}}v_{r_n}^*\mathrm{d}s\mathrm{d}s \\ &= \sum_{m=1}^{M_s}\sum_{n=1}^{M_s}\frac{\rho_{\mathrm{air}} c_{\mathrm{air}}}{2}\frac{k^2}{2\pi}v_{r_m}\frac{\sin(k\cdot r_{mn})}{k\cdot r_{mn}}v_{r_n}^*(S_m)^2, \end{aligned} \tag{32}$$

where S_m denotes the area of the discrete element, which is assumed as equal. r_{mn} denotes the distance between the center of the mth element with the center of the nth element. v_{r_m} denotes the vibration velocity at the center of the mth element. The above radiated acoustic power expression can also be written as follows:

$$\prod_r = \sum_m^{M_s} \sum_n^{M_s} v_{r_m} R_{\mathrm{mn}} v_{r_n}^*, \tag{33}$$

with

$$R_{\mathrm{mn}} = \begin{cases} \dfrac{k^2 (\Delta s)^2 \rho_{\mathrm{air}} c_{\mathrm{air}}}{4\pi} \dfrac{\sin(k \cdot r_{\mathrm{mn}})}{k \cdot r_{\mathrm{mn}}} & m \neq n, \\ \dfrac{k^2 (\Delta s)^2 \rho_{\mathrm{air}} c_{\mathrm{air}}}{4\pi} & m = n, \end{cases} \tag{34}$$

The sound transmission loss (STL) of the stiffened double panel-cavity coupled system can be written as follows:

$$\mathrm{STL} = 10 \log_{10}\left(\frac{\prod_{\mathrm{in}}}{\prod_r}\right). \tag{35}$$

3. Numerical Results and Discussions

In this section, the validation of the numerical results and the influence of some key parameters on vibro-acoustic will be carried out. For convenience, three panels have the same material properties and medium constants in two acoustic cavities are assumed as the same, as shown in Table 1.

3.1. Model Validation. The convergence and correction of the current method are verified in this subsection. Table 2 presents the first eight natural frequencies of the stiffened double panel-cavity coupled system. In this analysis, the medium constants in two acoustic cavities, the geometric parameters, and the material properties of all panels are given in Table 1. Except for panel-cavity coupled surfaces, other inner surfaces of two acoustic cavities are perfectly rigid. The structural coupled positions are considered rigid connections, where the coupled springs are set to infinity (5×10^9). Other boundary conditions of stiffened double panel structure are simply supported. The truncation numbers of pressure functions are set as $M_x = M_y = M_z = 4$. The ANSYS results are calculated in commercial software ANSYS with an element size of 0.02 m × 0.02 m. All panel structures and two acoustic cavities are modeled by SHELL63 and FLUID30 elements, respectively. Numerical results show that this method has good accuracy and fast convergence.

Based on the above frequency validations, we can obtain the vibration mode shapes of the stiffened panel structure in the stiffened double panel-cavity coupled system, as shown in Figures 3 and 4. It is easily seen that the vibration mode shapes of the stiffened double panel structure calculated by the current method agree well with those by the ANSYS from these figures. The differences between the modal shapes obtained by the current method and ones obtained by the ANSYS are mainly due to the selection of color map. In the first eight modes, the 1st, 6th, and 7th modes are mainly concentrated on the stiffened plate, and the rest modes are concentrated on the upper and lower plates. It is worth noting that all panels in the stiffened panel structure are coupled with acoustic cavities. Therefore, the sound pressure mode shapes of two acoustic cavities in the stiffened double panel-cavity coupled system should be considered. Figure 5 presents some sound pressure mode shapes of two acoustic cavities in the stiffened double panel-cavity coupled system. From this figure, it is easily seen that the sound pressure mode shapes of two acoustic cavities in the stiffened double panel-cavity coupled system calculated by the current method can agree with those by the ANSYS. It is worth noting that structure control modes are more than acoustic cavity control modes. For example, the 5th mode belongs to acoustic cavity control mode, while the rest of the first eight order modes belong to structure control mode.

Table 1: Geometric parameters and material properties of the stiffened double panel-cavity coupled system.

Object	Value (units)
Acoustic cavity, a (Lxa × Lya × Lza)	0.5 m × 0.6 m × 0.8 m
Acoustic cavity, b (Lxb × Lyb × Lzb)	0.5 m × 0.6 m × 0.8 m
The thickness of panels, h	0.004 m
The density of panels, ρ	7,800 kg/m^3
Young's modulus of panels, E	2.16×10^{11} Pa
Poisson's ratio of panels, μ	0.28
The density of cavity mediums, ρ_{air}	1.21 kg/m^3
The acoustic velocity of cavity mediums, c_{air}	344 m/s

Assume that the point ($x_1 = 0.7$ and $y_1 = 0.3$) on panel 1 is acted by the point force, whose amplitude is equal to 1 N, and its direction points to the negative direction of z_1. The damping ratios of all panel structures and acoustic cavities are set as 0.015. The reference values for the vibration velocity of panel structures and the acoustic pressure in cavities are 10^{-9} m/s and 2×10^{-5} Pa, respectively. Figures 6–10 show vibration velocity responses at some points on panel structures under simply supported boundary conditions. Figures 9 and10 show the sound pressure responses at some points in acoustic cavities. It is easily seen that the vibration velocity responses at some points on all panels and the sound pressure responses at some points in acoustic cavities calculated by the current method are in good agreement with those calculated by the commercial software ANSYS from these figures.

3.2. Parameter Analysis. The geometric parameters and material properties used for parameter analysis in this subsection are the same as those in previous examples, and the boundary conditions of the stiffened double panel structure and acoustic cavities remain unchanged. The

Table 2: First eight natural frequencies of the stiffened double panel-cavity coupled system.

Mode no	Natural frequencies (Hz)						
	$M=N=7$	$M=N=8$	$M=N=9$	$M=N=10$	$M=N=11$	$M=N=12$	ANSYS
1	51.963	51.890	51.471	51.436	51.317	51.295	50.555
2	73.439	73.211	71.734	71.638	71.506	71.441	70.141
3	79.493	79.302	78.021	77.941	77.763	77.711	76.159
4	85.457	84.708	84.709	84.436	84.437	84.279	83.801
5	86.783	86.054	86.055	85.791	85.788	85.637	85.127
6	113.23	113.20	112.57	112.57	112.08	111.99	109.52
7	130.05	130.02	129.74	129.75	129.58	129.59	128.58
8	157.83	157.82	154.68	154.71	154.25	154.29	151.56

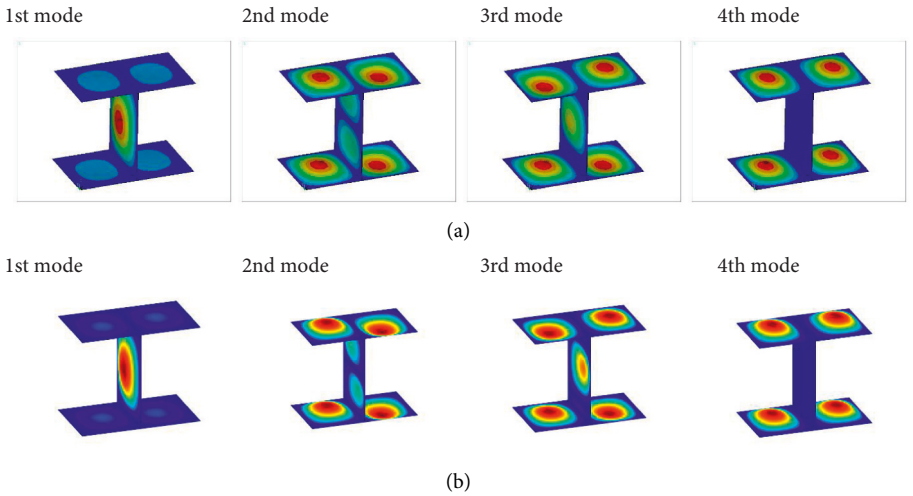

Figure 3: First four vibration mode shapes of the stiffened panel structure in the stiffened double panel-cavity coupled system: (a) results from ANSYS and (b) results from the current method.

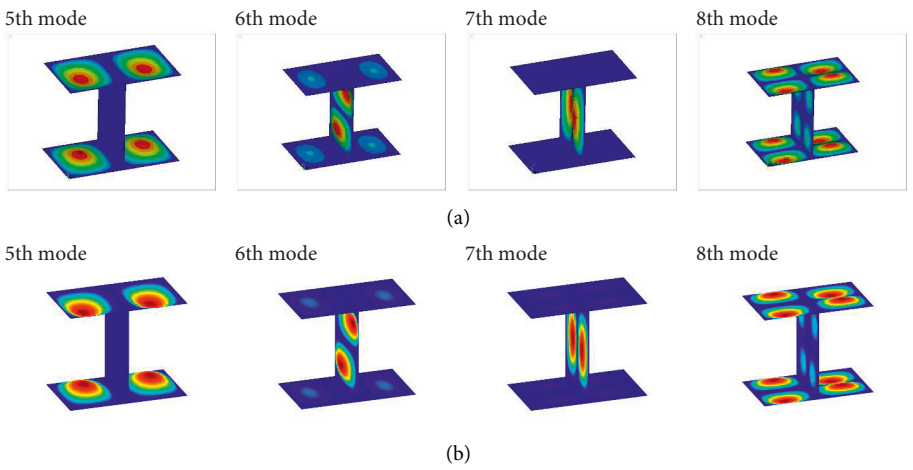

Figure 4: The 5th–8th vibration mode shapes of the stiffened panel structure in the stiffened double panel-cavity coupled system: (a) results from ANSYS and (b) results from the current method.

specific parameters of vibro-acoustic behavior can be studied with only changing corresponding parameters, such as thickness, length, material properties, or boundary conditions. The effects of the stiffener (panel 3) on the natural frequencies, responses, and sound transmission loss (STL) of the panel-cavity coupled system are studied in detail. When considering the influence of boundary springs on the vibration behavior, the response, and STL of the stiffened double panel-cavity coupled system, the stiffness amplitudes of all normal springs at the edges $y=0$ and $y=Ly3$ of the stiffener are equal to k_{vs}, while the stiffness amplitudes of other springs remain unchanged.

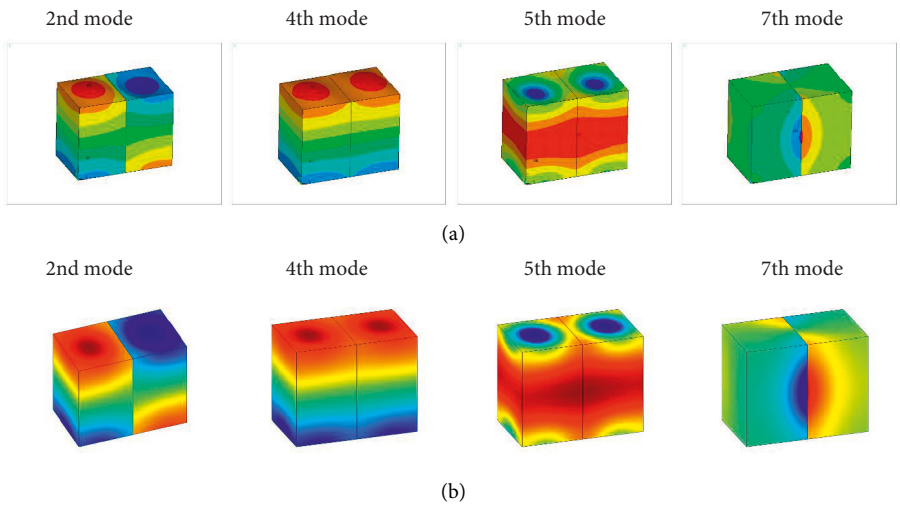

Figure 5: Some sound pressure mode shapes of two acoustic cavities in the stiffened double panel-cavity coupled system: (a) results from ANSYS and (b) results from the current method.

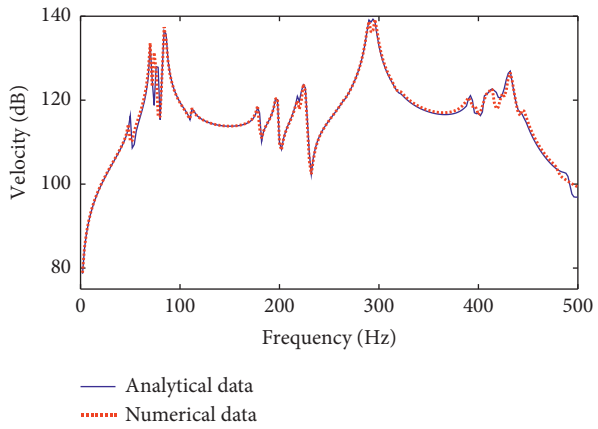

Figure 6: Vibration velocity response at the position ($x_1 = 0.8$ m, $y_1 = 0.1$ m) on the surface of panel 1.

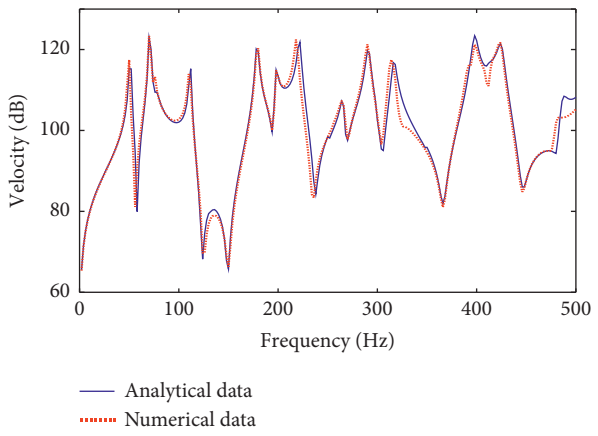

Figure 8: Vibration velocity response at the position ($x_3 = 0.1$ m, $y_3 = 0.1$ m) on the surface of the stiffener.

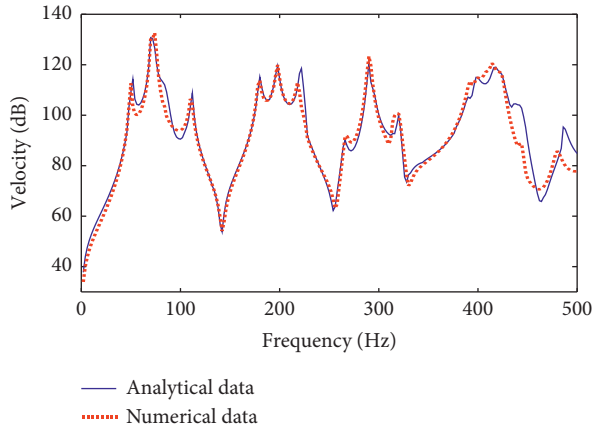

Figure 7: Vibration velocity response at the position ($x_2 = 0.2$ m, $y_2 = 0.1$ m) on the surface of panel 2.

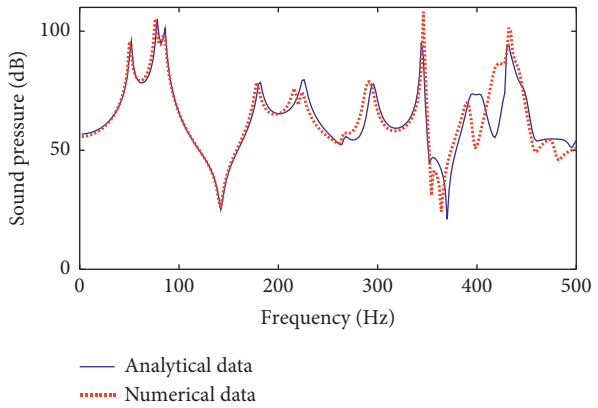

Figure 9: Sound pressure response at the position ($x_a = 0.3$ m, $y_a = 0.3$ m, and $z_a = 0.4$ m) in the acoustic cavity a.

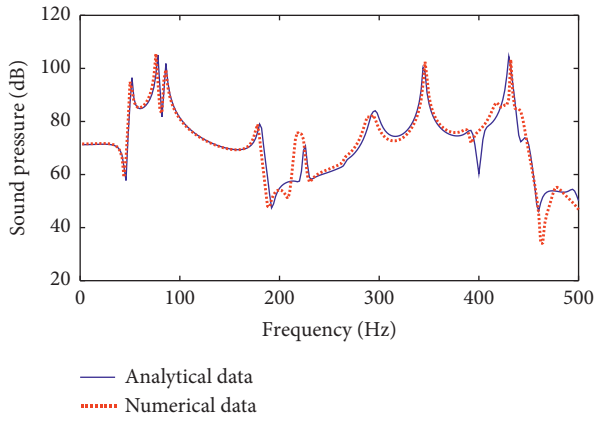

FIGURE 10: Sound pressure response at the position ($x_b = 0.1$ m, $y_b = 0.3$ m, and $z_b = 0.4$ m) in the acoustic cavity b.

3.2.1. Natural Vibration Behavior Analysis. Table 3 presents the first seven natural frequencies of the stiffened double panel-cavity coupled system with different thicknesses of the stiffener. In this analysis, the thickness h_3 is set as 0.001 m, 0.002 m, 0.004 m, 0.006 m, and 0.008 m, respectively. From this figure, it is easily seen that the vibration frequencies can be affected by the thickness h_3, and the natural frequencies increase monotonously with the increasing thickness h_3. The reason for this phenomenon is that the bending stiffness of the stiffener increases faster than the mass with the increase of thickness h_3.

Table 4 presents the first seven natural frequencies of the stiffened double panel-cavity coupled system with the different lengths of the stiffener. In this analysis, the length $Lx3$ is set as 0.2 m, 0.3 m, 0.4 m, 0.6 m, and 0.8 m, respectively. From this figure, it is easily seen that the natural frequencies decrease monotonously with the increasing thickness. The natural frequencies of the stiffened double panel-cavity coupled system depend mainly on the stiffened double-panel structures, and the increase of the length $Lx3$ leads to the increase of flexibility of the stiffener. As a result, the frequencies of the system decrease monotonously.

Table 5 presents the first seven natural frequencies of the stiffened double panel-cavity coupled system with different stiffness amplitudes of boundary springs at the $y = 0$ and $y = Ly3$ boundary edges. In this analysis, the stiffness amplitude of the boundary spring k_{vs} is set as 1E1, 1E3, 1E5, 1E7, or 1E9. It can be seen from this figure that the spring stiffness coefficient has an obvious influence on the natural frequencies of the structure within a certain range, but beyond this range, the influence is weak. For example, the natural frequencies increase slowly with the increasing the stiffness amplitude of the boundary spring k_{vs}, when k_{vs} is smaller than 1E5. However, the stiffness amplitude of the boundary spring k_{vs} can result in an obvious increase of natural frequencies when $1E5 \le k_{vs} \le 1E7$. A certain range can be determined by the stiffness matrix of the system. Small spring stiffness coefficients can be considered an unconstrained boundary condition, while large spring stiffness coefficients can be considered a fully constrained boundary condition.

3.2.2. Vibration Velocity Response and Sound Pressure Response Analyses. In this subsection, the vibration velocity response and pressure response analyses are presented. The medium constants of the acoustic cavity, the geometric parameters, and the material properties of panel structures are the same as those used in Figures 6–10. The amplitude of the point force, the direction of the point force, and the position acted by the point force remain unchanged. In other words, the corresponding vibro-acoustic model of the stiffened double panel-cavity coupled system in Figures 6–10 is used in this subsection.

Figures 11–13 present the influence of the thickness, length, boundary conditions, and material properties of the stiffener on the vibration velocity response at the point $x_2(x_2 = 0.2$ m, $y_2 = 0.1$ m) on panel 2 and sound pressure response at the point ($x_a = 0.3$ m, $y_a = 0.3$ m, and $z_a = Lza$) in the acoustic cavity a. Except for the object being analyzed, the others remain unchanged in these figures. For example, the thickness h_3 that is equal to 0.002 m, 0.004 m, or 0.008 m is selected for the thickness analysis in Figure 11. The Al, ZrO_2, and Al_2O_3 material properties used in Figure 14 are respectively: $E_{Al} = 7 \times 10^9$ Pa, $\mu_{Al} = 0.3$, and $\rho_{Al} = 2{,}700$ kg/m^3; $E_{ZrO_2} = 200 \times 10^9$ Pa, $\mu_{ZrO_2} = 0.3$, and $\rho_{ZrO_2} = 5{,}700$ kg/m^3; and $E_{Al_2O_3} = 380 \times 10^9$ Pa, $\mu_{Al_2O_3} = 0.3$, and $\rho_{Al_2O_3} = 3{,}800$ kg/m^3. Some remarks can be given from these figures: (1) with the increase of the thickness of the stiffened panel, the resonance peaks of vibration velocity and sound pressure become less, and the resonance peaks move to higher frequencies. However, some peak values of sound pressure response remain unchanged with the increase in thickness. (2) When the height of the cavity and the length of the stiffened panel increase at the same time, the number of the response peaks of the vibration velocity of the bottom panel and sound pressure increases, and the sound pressure response become weak in general. (3) When the stiffness coefficients of the boundary springs change from 1E1 to 1E5, there is no obvious change in the vibration velocity response and acoustic pressure response. When the stiffness coefficients of the boundary springs increase from 1E5 to 1E9, some resonance peaks of the velocity response and sound pressure move to higher frequencies. (4) The response curve for the Al material is closer to the response curve for the ZrO_2 material than one for the Al_2O_3 material. The reason for the above phenomenon may be that the change of the geometric parameters and properties of the stiffened panel can cause the change of some natural frequencies; as a result, some vibration velocity and sound pressure response peaks will move. The change of acoustic cavity height can result in the distance between the top panel with the sound pressure response point in the acoustic cavity varying, and then the amplitude of the sound transmission loss will change.

The acoustic cavity plays an important role in the panel-cavity coupled system. Therefore, the effects of the acoustic cavity on the vibration velocity and sound pressure should be investigated. The previous response analysis model of the stiffened double panel-cavity coupled system remain unchanged, and some parameters of acoustic cavities are changed for the next response analyses. Figure 15 presents the vibration velocity and sound pressure responses of the

Table 3: First seven natural frequencies of the stiffened double panel-cavity coupled system with the different thickness of the stiffener.

Mode	Natural frequencies (Hz)				
	$h_3 = 0.001$ m	$h_3 = 0.002$ m	$h_3 = 0.004$ m	$h_3 = 0.006$ m	$h_3 = 0.008$ m
1	28.956	34.529	51.435	66.297	77.855
2	32.128	57.074	71.640	78.322	83.472
3	32.382	65.343	77.945	84.449	84.454
4	47.504	70.485	84.440	85.798	85.801
5	54.079	70.618	85.790	89.355	101.10
6	66.829	84.411	112.56	150.29	161.50
7	68.532	85.770	129.74	159.13	161.55

Table 4: First seven natural frequencies of the stiffened double panel-cavity coupled system with different lengths of the stiffener.

Mode	Natural frequencies (Hz)				
	$Lx3 = 0.2$ m	$Lx3 = 0.3$ m	$Lx3 = 0.4$ m	$Lx3 = 0.6$ m	$Lx3 = 0.8$ m
1	77.969	74.750	72.187	63.692	51.435
2	78.370	76.336	75.047	73.312	71.639
3	84.681	84.688	84.658	84.563	77.943
4	88.875	87.553	86.872	86.164	84.438
5	154.72	154.52	137.34	87.783	85.788
6	157.60	156.63	153.99	145.49	112.56
7	160.95	161.22	156.09	155.41	129.74

Table 5: First eight natural frequencies of the stiffened double panel-cavity coupled system with the boundary springs of the stiffener.

Mode	Natural frequencies(Hz)				
	$k_{vs} = 1E1$	$k_{vs} = 1E3$	$k_{vs} = 1E5$	$k_{vs} = 1E7$	$k_{vs} = 1E9$
1	34.864	34.902	38.046	50.814	51.425
2	44.971	45.056	52.671	71.464	71.629
3	69.460	69.463	69.701	77.762	77.938
4	75.465	75.470	75.935	84.005	84.406
5	83.956	83.956	83.956	85.784	85.786
6	85.784	85.784	85.784	110.70	112.54
7	93.866	93.880	95.204	123.16	129.68

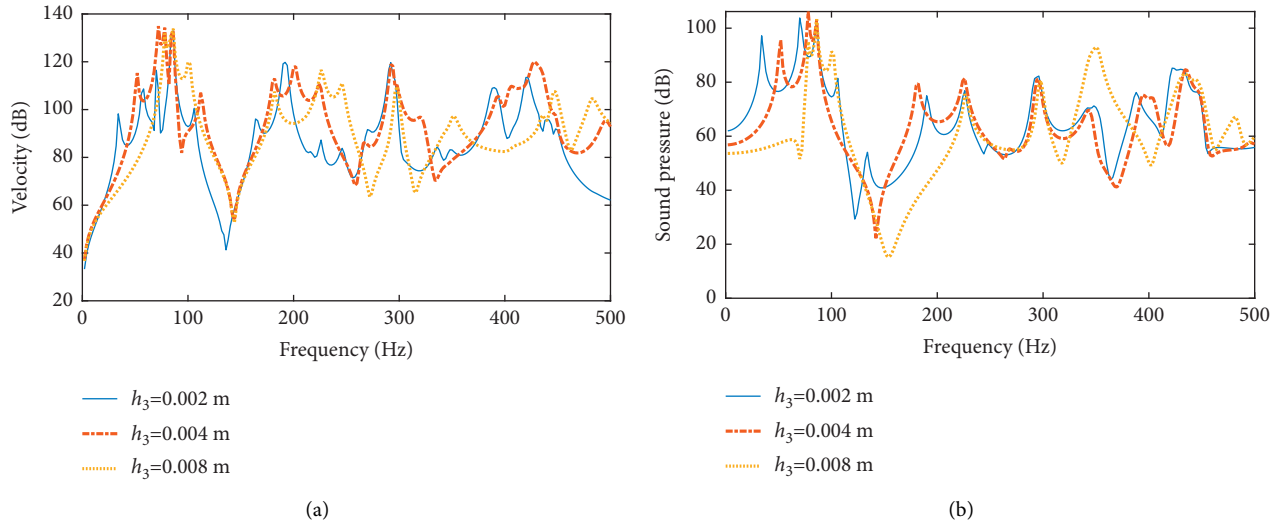

Figure 11: Vibration velocity response at the point on the surface of panel 2 and sound pressure response at the point in the acoustic cavity a with different h_3: (a) vibration velocity response and (b) sound pressure response.

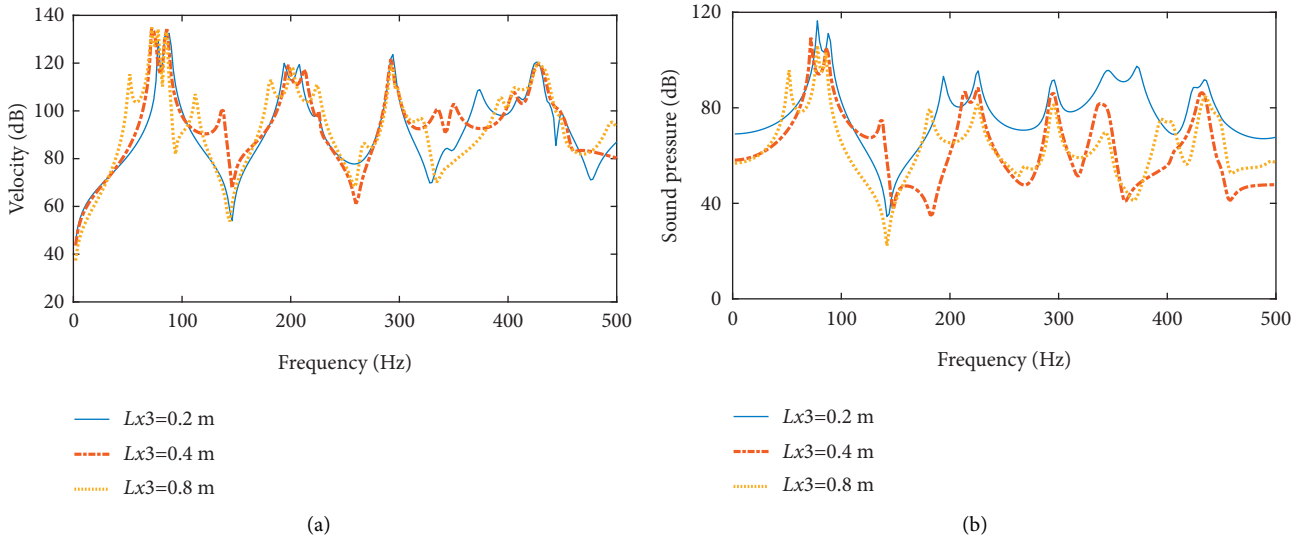

FIGURE 12: Vibration velocity response at the point on the surface of panel 2 and sound pressure response at the point in the acoustic cavity a with different $Lx3$: (a) vibration velocity response and (b) sound pressure response.

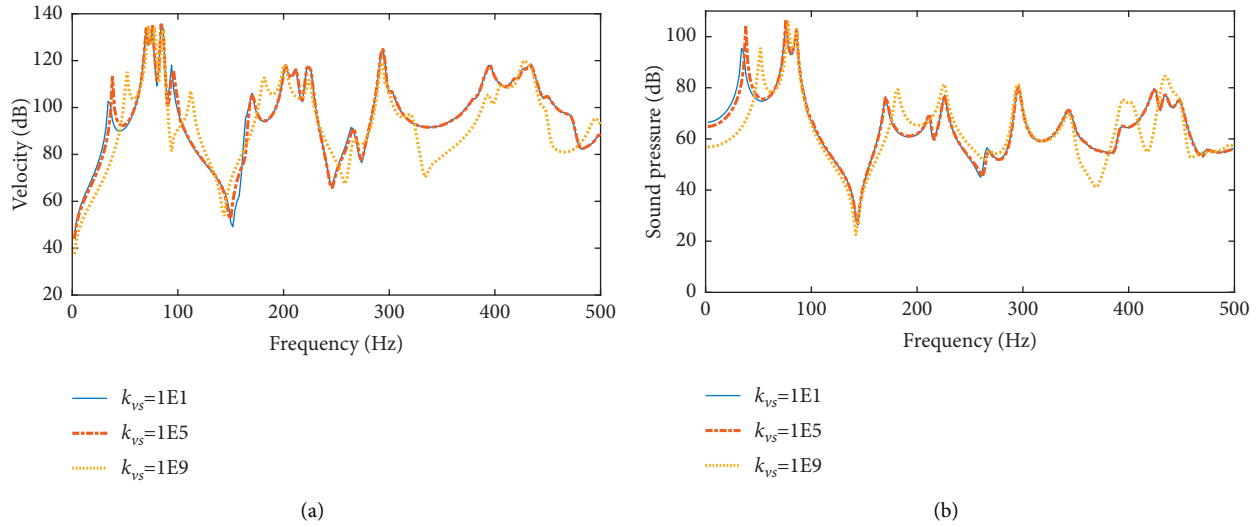

FIGURE 13: Vibration velocity response at the point on the surface of panel 2 and sound pressure response at the point in the acoustic cavity a with different k_{vs}: (a) vibration velocity response and (b) sound pressure response.

stiffened double panel-cavity coupled system with different acoustic cavity mediums. In this analysis, the acoustic cavity mediums, carbon dioxide (CO_2), air, and chlorine (Cl_2) gas are considered. Their medium constant are: $c_{CO_2} = 270$ m/s, $\rho_{CO2} = 1.83$ kg/m^3, $c_{air} = 343$ m/s, $\rho_{air} = 1.21$ kg/m^3, $c_{Cl_2} = 206$ m/s, and $\rho_{Cl_2} = 3.214$ kg/m^3. It is easily seen that the acoustic cavity medium has a weak influence on the vibration velocity, but it has a strong influence on sound pressure. Figure 16 presents the vibration velocity responses of the stiffened double panel structure with acoustic and vacuum cavities. It is easily seen that the acoustic cavity can cause a slight shift of resonance peaks, and the vibration velocity response curve with acoustic cavities has one more resonance peak than that without acoustic cavities at the $f = 85.6$ Hz. The reason for the above phenomenon is that the vibration velocity response is mainly determined by the structure, while the sound pressure response is mainly related not only to the structure but also to the medium constant of the acoustic cavity.

3.2.3. Sound Transmission Loss Analysis. In this subsection, the sound transmission loss analysis of the stiffened double panel-cavity coupled system under acoustic excitation is presented. The influence of the geometric parameters, material properties, and boundary conditions of the stiffened panel on the sound transmission loss of the stiffened double panel-cavity coupled system is investigated systematically. Then the influence of acoustic cavities on the sound transmission loss is considered. Except for the external

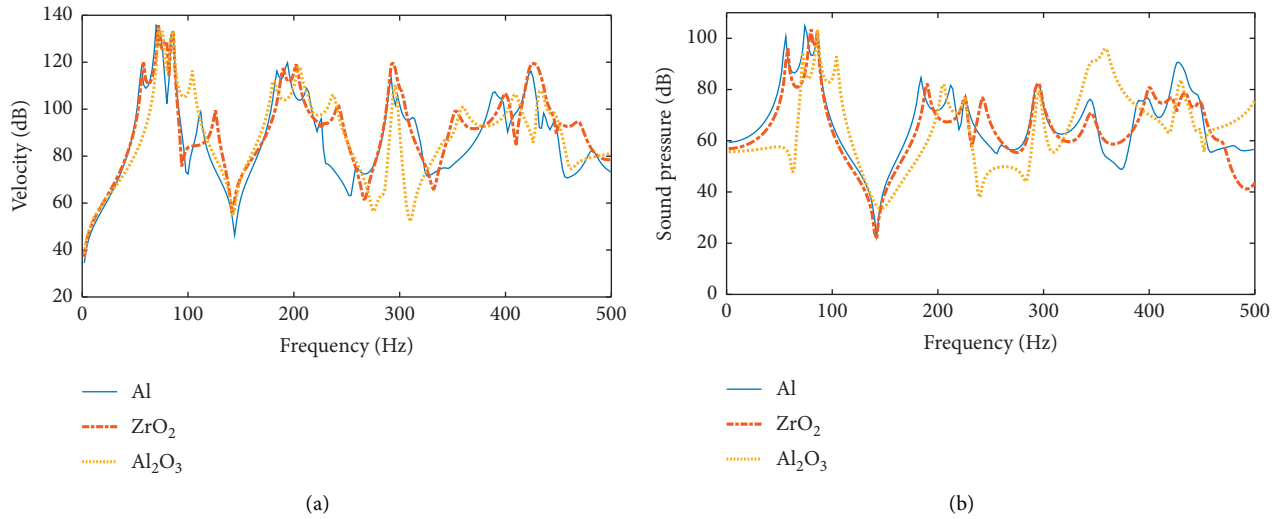

FIGURE 14: Vibration velocity response at the point on the surface of panel 2 and sound pressure response at the point in the acoustic cavity *a* with different material of the stiffener: (a) vibration velocity response and (b) sound pressure response.

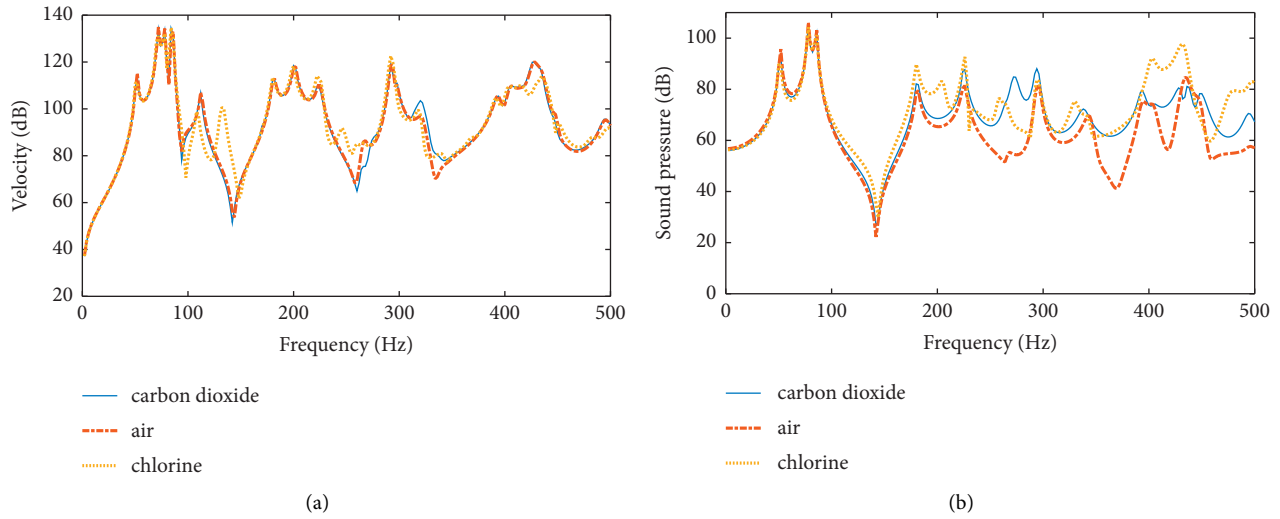

FIGURE 15: Vibration velocity response at the point on the surface of panel 2 and sound pressure response at the point in the acoustic cavity *a* with different acoustic cavity medium: (a) vibration velocity response and (b) sound pressure response.

excitation, other parameters of the system are consistent with the previous response analysis. The acoustic excitation with elevation angle $\varphi = \pi/4$, azimuth angle $\theta = \pi/4$, and the amplitude of the incident sound pressure $p_i = 1$ Pa is used for the STL calculation.

Figures 17–20 present the sound transmission loss of the stiffened double panel-cavity coupled system with various thicknesses, lengths, boundary conditions, and materials of the stiffener, respectively. Some remarks can be given from these figures: (1) the stiffened double panel-cavity coupled system with thicker stiffened panel has less number of sound transmission loss valleys of the sound pressure loss, and its valleys move to higher frequencies. (2) When the height of the cavity and the length of the stiffened panel increase at the same time, the number of sound transmission loss valleys increases, and the amplitude of sound transmission loss becomes bigger out of sound transmission loss valleys. (3) Some sound transmission loss valleys move to a higher frequency with the increasing stiffness coefficients of the boundary springs k_{vs} in a certain range. (4) The number of sound transmission loss valleys for the Al_2O_3 material is less than that for the Al material or ZrO_2 material. The reason for the above phenomenon may be that the stiffened panel has an obvious influence on the natural frequency of the system, and changing the parameters of the stiffened panel will result in the movement of some sound transmission loss valleys.

Figure 21 presents the sound transmission loss of the stiffened double panel-cavity coupled system with different acoustic cavity mediums. From the figure, it is easily seen that the sound transmission loss for the air acoustic cavity is close to one for the carbon dioxide acoustic cavity, and the system with a chlorine cavity medium has the smallest sound

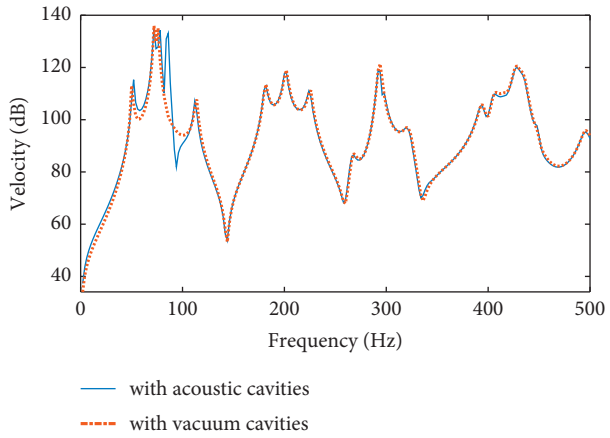

Figure 16: Vibration velocity response at the point on the surface of panel 2 with and without an acoustic cavity.

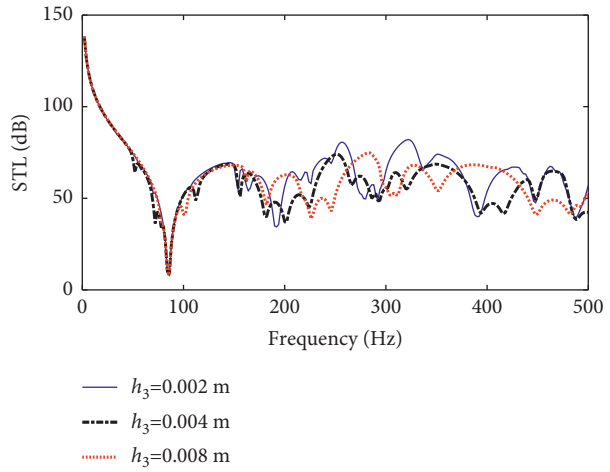

Figure 17: Sound transmission loss of the stiffened double panel-cavity coupled system with different thickness h_3.

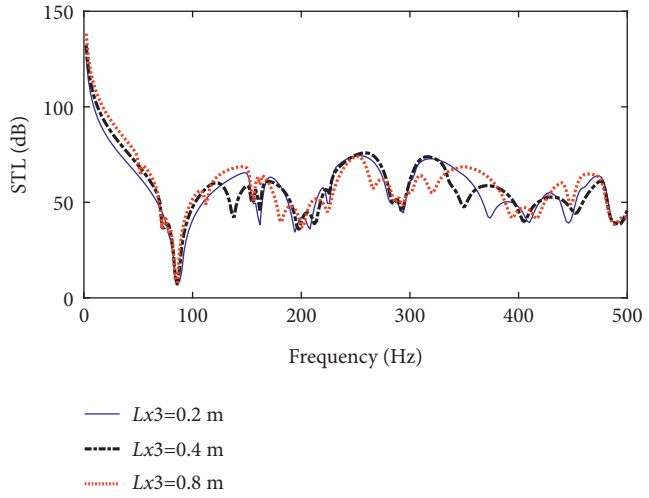

Figure 18: Sound transmission loss of the stiffened double panel-cavity coupled system with different length $Lx3$.

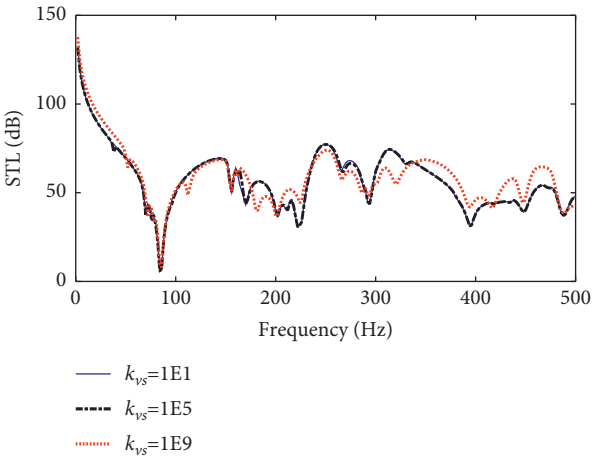

Figure 19: Sound transmission loss of the stiffened double panel-cavity coupled system with different stiffness amplitudes of boundary springs k_{vs}.

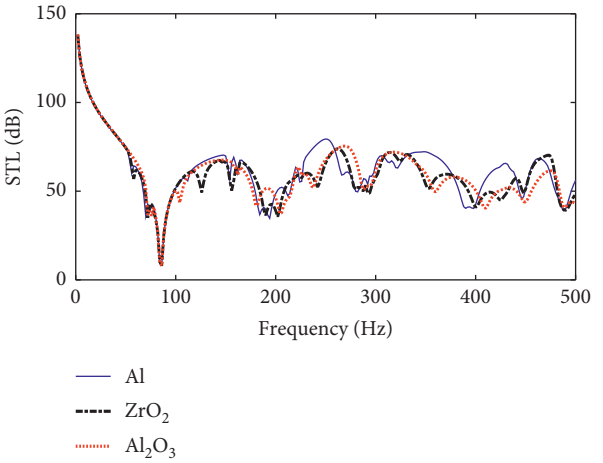

Figure 20: Sound transmission loss of the stiffened double panel-cavity coupled system with different materials of the stiffener.

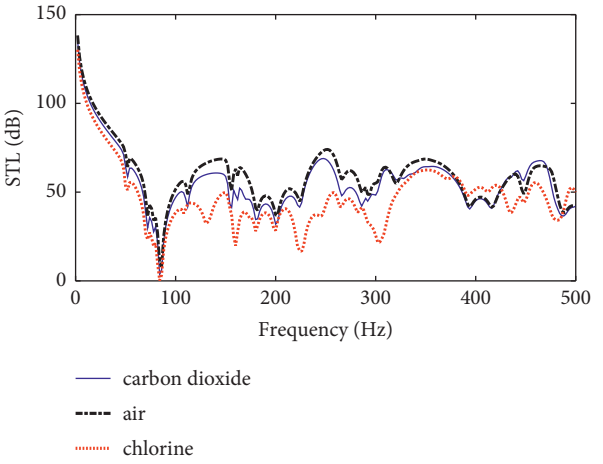

Figure 21: Sound transmission loss of the stiffened double panel-cavity coupled system with different acoustic cavity mediums.

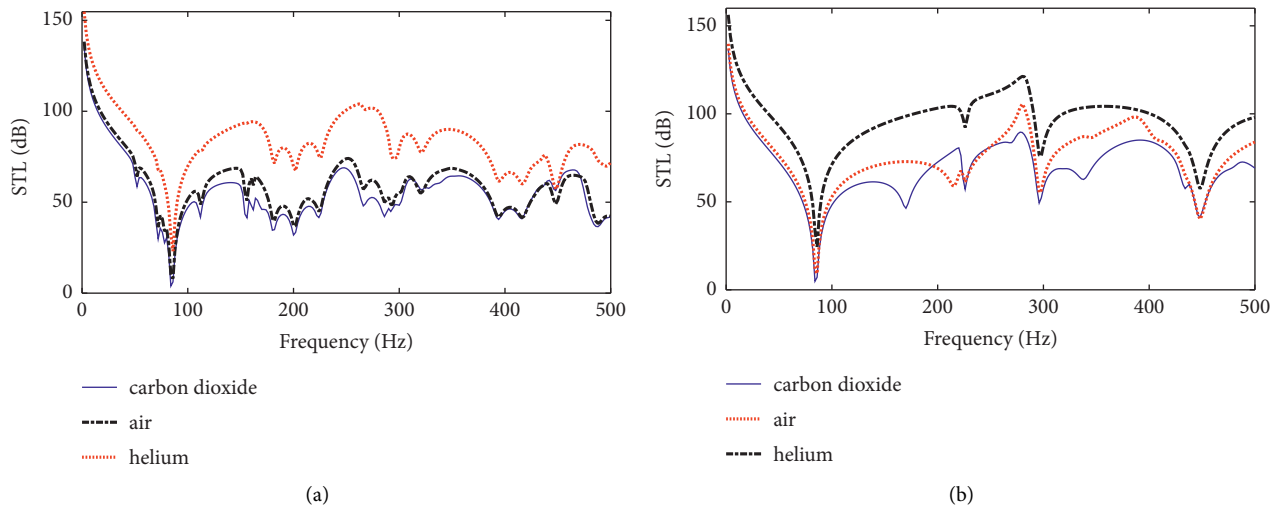

FIGURE 22: Sound transmission loss of the stiffened double panel-cavity coupled system with different acoustic cavity mediums: (a) acoustic excitation with elevation angle $\varphi = \pi/4$ and azimuth angle $\theta = \pi/4$ and (b) acoustic excitation perpendicular to panel 1.

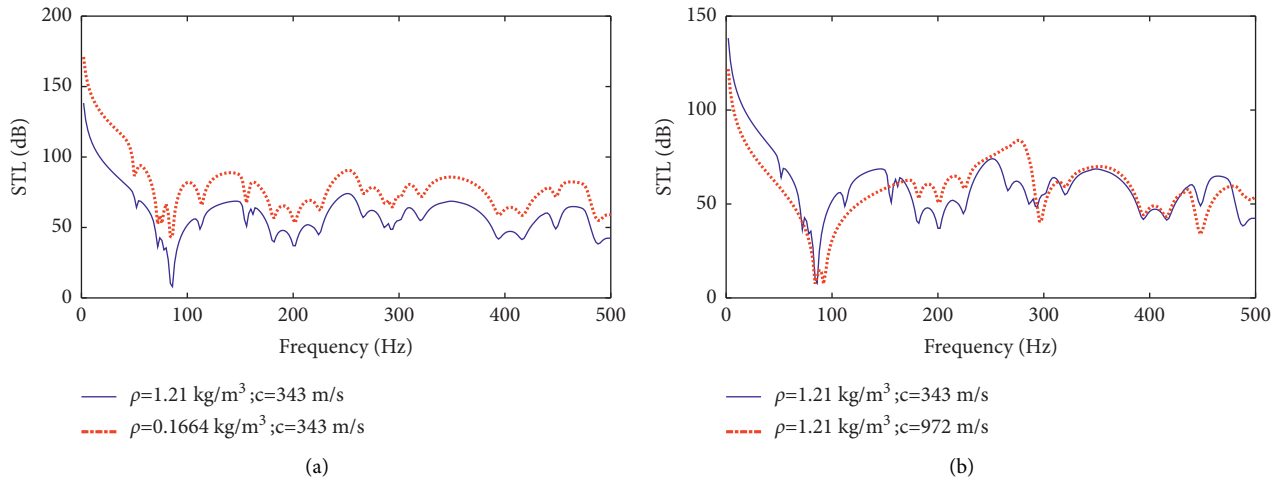

FIGURE 23: Sound transmission loss of the stiffened double panel-cavity coupled system with different acoustic cavity medium constant: (a) different density and (b) different acoustic velocity.

transmission loss of three acoustic cavity mediums. Then the helium with lower density and higher acoustic velocity is used to replace the chlorine in the cavity to analyze the sound transmission loss, as shown in Figure 22. The medium constants of the helium are defined as $c_{\text{helium}} = 972$ m/s and $\rho_{\text{helium}} = 0.1664\,\text{kg/m}^3$. In this analysis, the acoustic excitations at a certain angle and perpendicular to the top panel are considered. It is easily seen that the sound transmission loss of the system with helium is the biggest in the three cavity mediums. The number of sound transmission loss valleys of the system excited by acoustic excitation at a certain angle is larger than 1 by acoustic excitation perpendicular to the top panel. The reason may be that the structure control mode resonance frequencies of the system are more easily excited by the acoustic excitation at a certain angle, while the acoustic excitation perpendicular to the top panel can excite easily the acoustic cavity control mode resonance frequencies of the system.

Figure 23 presents the sound transmission loss of the system with different acoustic cavity medium constants, in which only one of the density and acoustic velocity of acoustic cavities in the system is changed. From Figures 22 and 23, it is easily seen that the density of the acoustic medium can affect the amplitude of sound transmission loss of the system, and the system with a smaller density acoustic medium has a bigger amplitude of sound transmission loss. The acoustic velocity of the acoustic medium can affect the acoustic cavity control mode resonance frequency; in other words, it can cause the movement of some sound transmission loss valleys.

In order to achieve better sound insulation, heat insulation, and heat preservation effects, the medium of the double panel-cavity system is often vacuumed in practical engineering, such as vacuum double-layer glass and heat insulation wall. Therefore, it is very necessary to study the double-panel cavity system with vacuum mediums.

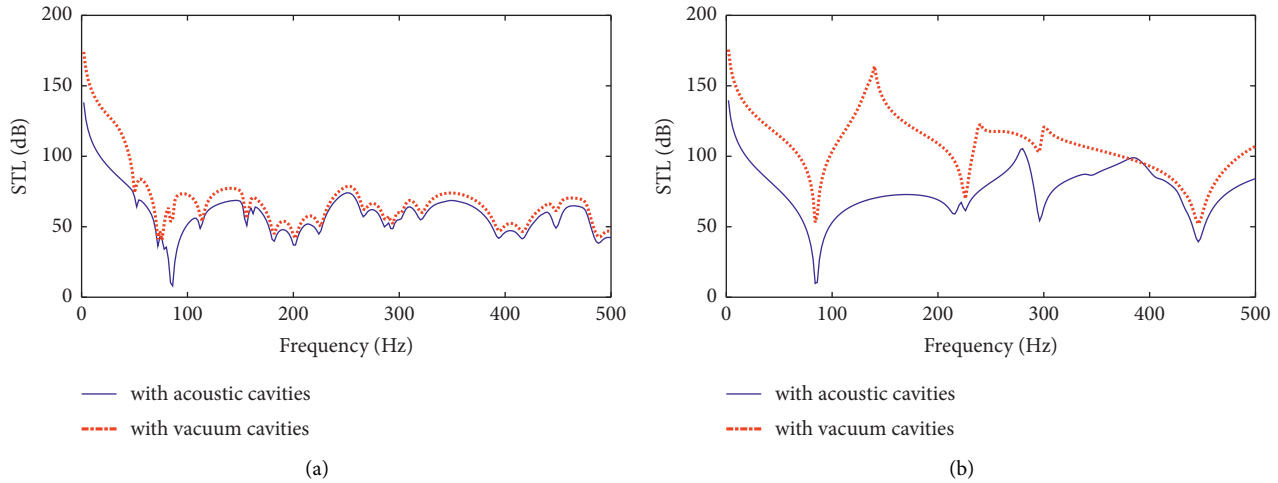

FIGURE 24: Sound transmission loss of the stiffened double panel structure with acoustic and vacuum cavities: (a) acoustic excitation at elevation angle $\varphi = \pi/4$ and azimuth angle $\theta = \pi/4$ and (b) acoustic excitation perpendicular to panel 1.

Figure 24 presents the sound transmission loss of the stiffened double panel structures with acoustic cavities and with vacuum cavities. The acoustic excitations at a certain angle and perpendicular to the top panel are considered in this analysis. From this figure, some remarks can be obtained: the stiffened double panel structure excited by the acoustic excitation at a certain angle has a bigger number of the sound transmission loss valleys than those excited by acoustic excitation perpendicular to the top panel. The difference between acoustic transmission loss of the system with acoustic cavities and with vacuum cavities for acoustic excitation perpendicular to the top panel is more obvious than one for acoustic excitation at a certain angle. The reason may be that the acoustic excitation at a certain angle can excite more structure control modes, and the corresponding sound transmission loss is mainly determined by structures in this case. Acoustic cavities can cause a slight shift of some valleys of the sound transmission loss of structures, and the amplitudes of sound transmission loss with vacuum cavities are bigger than those with acoustic cavities, especially at the low frequencies. It is worth noting that the sound transmission loss valley with acoustic cavities is smaller obviously than one with vacuum cavities, as the system with acoustic cavities has an acoustic cavity control mode at $f = 85.6$ Hz.

4. Conclusions

The vibro-acoustic behavior analysis model of an elastically restrained stiffened double panel-cavity coupled system has been proposed in this paper. The improved Fourier series method is used to describe the displacement functions of all panels and sound pressure functions in acoustic cavities. The unknown coefficients of displacement and sound pressure function are solved by the Rayleigh–Ritz method based on the energy principle of the structure-acoustic coupled system. The effectiveness and accuracy of the proposed model are validated by some comparisons in numerical examples. This method can overcome the differential discontinuities for various boundary and/or coupled conditions and be flexible with parameter analysis. However, it has limitations in the vibration behavior analysis of other irregular structure acoustical cavity coupled systems. From this study, some conclusions are as follows:

(1) The thickness, length, boundary condition, and material properties of the stiffened panel have an obvious influence on the natural vibration frequencies of the stiffened double panel-cavity coupled system.

(2) The geometric parameters and material properties of the stiffened panel can affect the vibration velocity response of the bottom panel and the sound pressure response in a cavity. The influence of the gas medium on the amplitude of acoustic pressure response in acoustic cavities is obvious, but that on the vibration velocity response of panels can be ignored.

(3) The structure control mode resonance frequencies of the system are more easily excited by the acoustic excitation at a certain angle, while the acoustic excitation perpendicular to the top panel can excite easily the acoustic cavity control mode resonance frequency of the system.

(4) The stiffened panel can affect the movement of the sound transmission loss valleys at structure control mode resonance frequencies; the acoustic velocity of acoustic cavities can cause the sound transmission loss valleys at acoustic cavity control mode resonance frequency to shift; and the density of acoustic cavity can affect the amplitude of the sound transmission loss.

Data Availability

No data were used to support the findings of the study.

Conflicts of Interest

The authors declare that they have no financial and personal relationships with other people or organizations that can

inappropriately influence our work, and there is no professional or other personal interest of any nature or kind in any product, service, and/or company that could be construed as influencing the position presented in, or the review of, this paper.

Acknowledgments

This work was supported by Guizhou Provincial Science and Technology Projects (ZK[2022] general 137).

References

[1] K. Li, L. Sheng, and D. Y. Zhao, "Investigation on vibration energy flow characteristics in coupled plates by visualization techniques," *Journal of Marine Science and Technology*, vol. 18, pp. 907–914, 2010.

[2] Y. Chen, G. Jin, J. Du, and Z. Liu, "Vibration characteristics and power transmission of coupled rectangular plates with elastic coupling edge and boundary restraints," *Chinese Journal of Mechanical Engineering*, vol. 25, no. 2, pp. 262–276, 2012.

[3] S. Yin, J. S. Hale, T. Yu, T. Q. Bui, and S. P. A. Bordas, "Isogeometric locking-free plate element: a simple first order shear deformation theory for functionally graded plates," *Composite Structures*, vol. 118, pp. 121–138, 2014.

[4] Y. Xue, G. Jin, H. Ding, and M. Chen, "Free vibration analysis of in-plane functionally graded plates using a refined plate theory and isogeometric approach," *Composite Structures*, vol. 192, pp. 193–205, 2018.

[5] C. Zhang, G. Jin, T. Ye, and Y. Zhang, "Harmonic response analysis of coupled plate structures using the dynamic stiffness method," *Thin-Walled Structures*, vol. 127, pp. 402–415, 2018.

[6] M. Chen, T. Ye, J. Zhang, G. Jin, and Z. Liu, "Isogeometric three-dimensional vibration of variable thickness parallelogram plates with in-plane functionally graded porous materials," *International Journal of Mechanical Sciences*, vol. 169, Article ID 105304, 2019.

[7] M. Chen, G. Jin, Y. Zhang, F. Niu, and Z. Liu, "Three-dimensional vibration analysis of beams with axial functionally graded materials and variable thickness," *Composite Structures*, vol. 207, pp. 304–322, 2019.

[8] J. M. Navarro, F. Jacobsen, J. Escolano, and J. J. López, "A theoretical approach to room acoustic simulations based on a radiative transfer model," *Acta Acustica united with Acustica*, vol. 96, no. 6, pp. 1078–1089, 2010.

[9] G. Jin, S. Shi, and Z. Liu, "Acoustic modeling of a three-dimensional rectangular opened enclosure coupled with a semi-infinite exterior field at the baffled opening," *Journal of the Acoustical Society of America*, vol. 140, no. 5, pp. 3675–3690, 2016.

[10] S. Shi, G. Jin, B. Xiao, and Z. Liu, "Acoustic modeling and eigenanalysis of coupled rooms with a transparent coupling aperture of variable size," *Journal of Sound and Vibration*, vol. 419, pp. 352–366, 2018.

[11] S. Shi, K. Liu, B. Xiao, G. Jin, and Z. Liu, "Forced acoustic analysis and energy distribution for a theoretical model of coupled rooms with a transparent opening," *Journal of Sound and Vibration*, vol. 462, Article ID 114948, 2019.

[12] A. London, "Transmission of reverberant sound through double walls," *Journal of the Acoustical Society of America*, vol. 22, no. 2, pp. 270–279, 1950.

[13] D. Takahashi, "Sound radiation from periodically connected double-plate structures," *Journal of Sound and Vibration*, vol. 90, no. 4, pp. 541–557, 1983.

[14] W. Kropp and E. Rebillard, "On the air-borne sound insulation of double wall constructions," *Acta Acustica united with Acustica*, vol. 85, pp. 707–720, 1999.

[15] F. C. Sgard, N. Atalla, and J. Nicolas, "A numerical model for the low frequency diffuse field sound transmission loss of double-wall sound barriers with elastic porous linings," *Journal of the Acoustical Society of America*, vol. 108, no. 6, pp. 2865–2872, 2000.

[16] L. Cheng, Y. Y. Li, and J. X. Gao, "Energy transmission in a mechanically-linked double-wall structure coupled to an acoustic enclosure," *Journal of the Acoustical Society of America*, vol. 117, no. 5, pp. 2742–2751, 2005.

[17] Y. Y. Li and L. Cheng, "Energy transmission through a double-wall structure with an acoustic enclosure: rotational effect of mechanical links," *Applied Acoustics*, vol. 67, no. 3, pp. 185–200, 2006.

[18] T. Y. Kam, C. H. Jiang, and B. Y. Lee, "Vibro-acoustic formulation of elastically restrained shear deformable stiffened rectangular plate," *Composite Structures*, vol. 94, pp. 3132–3141, 2012.

[19] J. P. Carneal and C. R. Fuller, "An analytical and experimental investigation of active structural acoustic control of noise transmission through double panel systems," *Journal of Sound and Vibration*, vol. 272, pp. 749–771, 2004.

[20] F. X. Xin, T. J. Lu, and C. Q. Chen, "Vibroacoustic behavior of clamp mounted double-panel partition with enclosure air cavity," *Journal of the Acoustical Society of America*, vol. 124, pp. 3604–3612, 2008.

[21] F. X. Xin, T. J. Lu, and C. Q. Chen, "Sound transmission through simply supported finite double-panel partitions with enclosed air cavity," *Journal of Vibration and Acoustics-Transactions of the ASME*, vol. 132, pp. 325-326, 2010.

[22] P. Raviprolu, N. Jade, and V. Balide, "Sound radiation characteristics of a rectangular duct with flexible walls," *Advances in Acoustics and Vibration*, p. 2016, 2016.

[23] L. Guo, J. Ge, and S. Liu, "Analysis of vibration and acoustic characteristics of a simply supported double-panel partition under thermal environment," *Shock and Vibration*, vol. 2020, pp. 1–11, 2020.

[24] Y. Y. Lee, "Free vibration analysis of a nonlinear panel coupled with extended cavity using the multi-level residue harmonic balance method," *Thin-Walled Structures*, vol. 98, pp. 332–336, 2016.

[25] M. Sadri and D. Younesian, "Nonlinear free vibration analysis of a plate-cavity system," *Thin-Walled Structures*, vol. 74, pp. 191–200, 2014.

[26] X. Zhang and W. L. Li, "Vibrations of rectangular plates with arbitrary non-uniform elastic edge restraints," *Journal of Sound and Vibration*, vol. 326, pp. 221–234, 2009.

[27] Y. Chen, G. Jin, M. Zhu, Z. Liu, J. Du, and W. L. Li, "Vibration behaviors of a box-type structure built up by plates and energy transmission through the structure," *Journal of Sound and Vibration*, vol. 331, pp. 849–867, 2012.

[28] J. T. Du, W. L. Li, Z. G. Liu, H. A. Xu, and Z. L. Ji, "Acoustic analysis of a rectangular cavity with general impedance boundary conditions," *Journal of the Acoustical Society of America*, vol. 130, pp. 807–817, 2011.

[29] J. T. Du, W. L. Li, H. A. Xu, and Z. G. Liu, "Vibro-acoustic analysis of a rectangular cavity bounded by a flexible panel with elastically restrained edges," *Journal of the Acoustical Society of America*, vol. 131, pp. 2799–2810, 2012.

[30] D. Shi, Z. Ying, and X. Lv, "Analysis of acoustic characteristics of arbitrary triangular prism and quadrangular prism acoustic cavities," *Shock and Vibration*, p. 2019, 2019.
[31] H. Zhang, D. Shi, Q. Wang, and S. Zha, "Vibro-acoustic analysis of the annular segment flexible plate coupled with an impedance walled enclosure," *Thin-Walled Structures*, vol. 131, pp. 205–222, 2018.
[32] S. X. Shi, G. Y. Jin, and Z. G. Liu, "Vibro-acoustic behaviors of an elastically restrained double-panel structure with an acoustic cavity of arbitrary boundary impedance," *Applied Acoustics*, vol. 76, pp. 431–444, 2014.
[33] W. L. Li, "Free vibrations of beams with general boundary conditions," *Journal of Sound and Vibration*, vol. 237, pp. 709–725, 2000.